The International Journal of Advanced Manufacturing Technology (2023) 129:5149–5165
https://doi.org/10.1007/s00170-023-12411-z

ORIGINAL ARTICLE

Surface treatments for the improvement of mechanical and cavitation resistance of Al 6082 alloy

Silvio Genna[1,2] · Claudio Leone[3,2] · Emanuele Mingione[4] · Gianluca Rubino[5]

Received: 1 July 2023 / Accepted: 28 September 2023 / Published online: 15 November 2023

Abstract

Nowadays, naval propellers are made in Ni-Al or Mn-Al bronzes, which are affected by high cavitation erosion. In this study, the possibility of adopting 6xxx alloy with different superficial treatments obtained through fluidised beds and laser surface texturing was investigated. 6xxx alloy series is known for its versatility due to an excellent mix of mechanical and physical properties, combined with ease of processing, welding, and good chemical resistance; however, its main drawback is low resistance to cavitation erosion. In this study, a total of 4 different surface treatments were produced and characterized such as fluidised bed coatings (Al2O3, S280) and laser textured samples (0–30% overlap). Moreover, the effect of a heat-treatment was evaluated for each kind of specimen analysed. The study was divided into two steps: in the first phase, the samples were morphologically and mechanically characterised through roughness measurements, micro-hardness, scratch, wear, and wettability tests. Successively, a modified ASTM-G32-10 standard was adopted to assess the cavitation erosion resistance; in particular, for each sample, mass and volume loss were analysed and compared to the as-built sample. Results showed a drastic reduction of the wear evaluated through pin-on-disk tests with the application of the high hardness coatings (Al2O3, S280) while a reduction of the cavitation erosion volume of about 20% lower was obtained through the best laser texturing treatment.

Keywords Cavitation erosion · Surface treatments · Fluidised bed · AA6082 · Coatings

1 Introduction

The 6000 series aluminium alloys are widely used in many industrial fields, such as the railway sector, production of fixtures, and marine industries due to excellent properties such as lightweight, good mechanical properties, easy weldability, and relatively good corrosion resistance [1–3].

✉ Emanuele Mingione
emanuele.mingione@unicusano.it

1 Department of Enterprise Engineering, University of Rome Tor Vergata, Via del Politecnico 1, 00133 Rome, Italy

2 CIRTIBS Research Centre, University of Campania Luigi Vanvitelli, via Roma 29, 81031 Aversa (CE), Italy

3 Department of Engineering, University of Campania Luigi Vanvitelli, via Roma 29, 81031 Aversa (CE), Italy

4 Department of Engineering, University Niccolò Cusano, Via Don Carlo Gnocchi 3, 00166, Rome (RM), Italy

5 Department of Economics, Engineering, Society, and Business Organization, Università degli Studi della Tuscia, Via del Paradiso, 47, 01100 Viterbo, Italy

In particular, AA 6082 is one of the alloys used for extruded parts in shipbuilding, like square and round bars/pipes, profiles of different shapes, and elements of the engine, such as propellers [4, 5]. Some of those parts are exposed to cavitation erosion caused by the impact of the sea waves and areas of depression that occur due to moving parts [6]. Cavitation erosion involves different kinds of interaction between physical processes such as metallurgical, chemical, mechanical, and hydrostatic ones. This phenomenon leads to surface deterioration and material loss due to the growth and collapse of bubbles, which are due to the local pressure fluctuations inside the flowing liquid around the surface of the parts. In detail, when there is a localized drop in pressure, the liquid reaches the vapour pressure and undergoes a phase change, forming bubbles (cavities) containing vapour. The cavitation bubble only lasts until it leaves the low-pressure zone; as soon as it returns to the zone of the still fluid, the bubble immediately implodes, forming a shock wave that impacts and erodes the surface of the part in contact.

To prevent or reduce erosion due to cavitation of the alloys, different methodologies have been studied and proposed, such as surface engineering methods, like the addition of the alloy of hydrophobic coatings [7, 8], or surface modification technologies.

The former is considered one of the possible solutions to the problem due to its excellent resistance to corrosion and self-cleaning properties. According to the literature, the improvement in corrosion resistance of hydrophobic coatings is attributed to the formation of an air cushion on the surface of a part, which can prevent or control corrosion processes [9, 10]. Several techniques allow the production of hydrophobic coatings, such as electrochemical deposition [11], chemical vapour deposition [12], sol-gel processing [13, 14], emulsion [15], fluidised bed [16], and plasma method [17]. However, in all cases, before the coating process, the surface needs to be properly treated to allow an adequate coating adhesion.

Surface modification technologies improve the wear property of metallic materials through plastic deformation or by changing the surface's wettability due to morphological changes. The first mechanism induces grain refinement and compressive residual stress, which is opposite to the stress derived from the bubble's explosion that causes the removal of material. Those technologies include shot peening [18, 19], laser shock peening [20, 21], cold rolling [22], and equal-channel angular pressing [23, 24]. Due to both the compressive residual stresses and refined grains generated by the processes, the fatigue behaviour, corrosion resistance, and wear characteristics of metallic materials are improved.

To obtain a surface modification on metals, one of the most promising alternatives is given by laser surface treatments, to achieve phase transformation [25, 26], melting and alloying [27, 28], powder densification [29, 30], texturing [31, 32], and cladding [33, 34]. Those methodologies are simple methods in surface modification, which enhance surface properties via homogenization and refinement of the microstructure and have been widely studied to improve the cavitation erosion resistance of different alloys [35, 36].

Man et al. [37] made a laser surface alloying of SiC/Si_3N_4 on AA6061 aluminium alloy by using a 2-kW CW Nd-YAG laser. The cavitation erosion resistance was improved by three times compared to the AA6061 alloy whereas there was no significant improvement in the specimen alloyed with 100% SiC (AA6061-SiC). Kwok et al. [38] performed a surface modification of austenitic stainless steel S30400 and super duplex stainless steel S32760 by laser surface melting using a 2 kW continuous wave Nd-YAG laser. In a series of 4-h cavitation tests, the cavitation erosion resistance of laser-melted S31603 with 50% overlapping of melted tracks was found to be improved by 22% at 23 °C compared with the as-received specimens.

One of the less exploited alternatives to increase the resistance to cavitation erosion consists of laser texturing. There are different studies which showed the change in wettability of the surface due to different textures. Genna et al. [31] used a ns-pulsed laser to ablate different patterns on the surfaces of AISI 304 samples and evaluated the effects of the process parameters on the wettability with a multilevel factorial design. The results indicate a significant change in the wettability due to the produced textures on the sample surfaces, with contact angles in the range of 30–110°. Ponticelli et al. [39] made a laser surface texturing with a nanosecond-pulsed laser on the surfaces of AISI 304 samples, changing the laser processing parameters, and obtained significant changes of the contact angle in the range 24–121° due to the different textures.

In this paper, two different surface treatment technologies to improve the mechanical and cavitation erosion resistance of Al6082 alloy have been studied: laser surface texturing and fluidised bed techniques. In particular, laser texturing was performed with two different pulse overlaps (0–30%), while two different coatings, alumina (Al_20_3) and S280 steel, were produced by fluidised bed technology. In addition, to improve the diffusion of the material coatings into the substrate and to remove the residual stresses, the coated samples were subjected to a thermal treatment.

The samples were morphologically and mechanically characterised through roughness measurements, microhardness, scratch, and wettability tests. Wear tests were also performed in order to assess the effectiveness of the realised treatments on the wear behaviour; in particular, for each sample, volume loss and surface maps were analysed and compared. Successively, a modified ASTM-G32-10 standard [40], widely discussed in the literature [41–45], was adopted to test the cavitation erosion resistance; in particular, the differences between the wear obtained with tests carried out with a standard tribometer and the wear obtained by cavitation erosion were underlined.

2 Materials and methods

2.1 Material

The studied material is 6082 aluminium alloy (AA6082). In Table 1, the chemical and mechanical properties are reported. In order to verify the effectiveness of the treatments, the samples were made in accordance with the ASTM-G32-10 standard [40]; an image of the samples is shown in Fig. 1.

2.2 Equipment

The laser treatments were performed adopting a 30W Yb: YAG fiber source (model YLP-RA30-1-50-20-20 supplied by IPG), equipped with a galvanometric scanning head (supplied by LASIT SpA) and a flat focus (LINOS F-Theta) with a focal length of 160 mm. In Fig. 2 and Table 2, the schematic and the main characteristics of the laser system are shown. It is worth noting that the source used operates in pulsed wave mode; for this reason, by suitably adjusting the pulse frequency and the scanning speed, it is possible to change the spatial overlap of the pulses (defined as spot overlap).

The system is managed through a PC that allows controlling the laser power (P) (through the power supply current of the pumping diodes), the pulse frequency (f), the repetition number (R) (i.e. the number of times the operation is performed), the scan speed (S) and the scan strategy. The latter represents the set of lines along which the laser beam is

Table 1 Chemical composition and mechanical properties of 6082 aluminium alloy

Chemical composition of 6082 aluminium alloy (%)*							
Si	Fe	Cu	Mn	Mg	Zn	Ti	Others
0.70-1.30	0.50	0.10	0.40–1.00	0.60–1.20	0.20	0.10	0.15
Mechanical properties of 6082 aluminium alloy**							
Thickness (mm)		Rp 0.2 (MPa)		*R* (MPa)	HBV		
From	*To*						
0.4	1.5	260		310	94		
1.5	6.0	260		310	94		
3.0	6.0	260		310	94		
6.0	12.5	255		310	91		

*Indicated in mass percentage

**Properties calculated at environmental condition

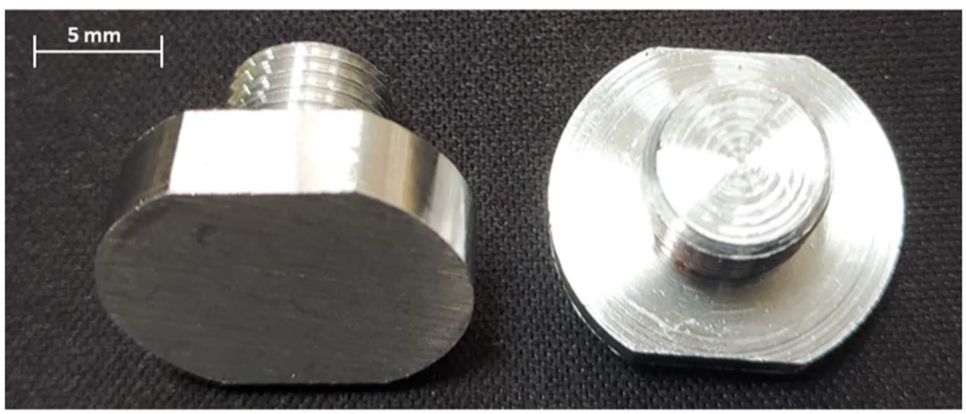

Fig. 1 Samples made according to ASTM-G32-10 standard [40]

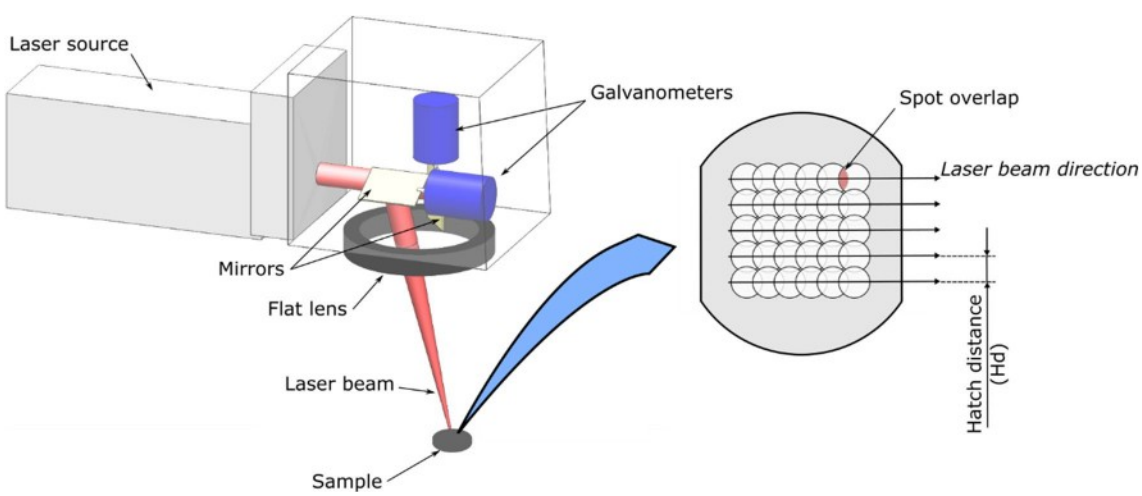

Fig. 2 Schematic of the laser system used

Table 2 Laser system characteristics

Property	Symbol	Value	UM
Wavelength	λ	1064	nm
Mode	--	PW	--
Max power	P	30	W
Pulse repetition rate	f	30–80	kHz
Pulse duration	D	50	ns
Maximum pulse energy (at 30 kHz)	Ep	1	mJ
Maximum peak power (at 30 kHz)	Pp	20	kW
Quality of the laser beam	TEM	00	--
	M^2	1.2–1.5	--
Beam diameter at the focus point	d	80	µm
Work area (with 160 mm lens)	A	100 × 100	mm^2
Maximum scan speed	v	5000	mm/s

moved to cover the entire area to be processed; the strategy, therefore, here represents the distance between two successive scanning lines (Hatch distance, Hd).

The steel and alumina coatings were performed in the fluidised bed device reported in Fig. 3. The system includes an air supply system, a vertical fluidization column in polymethylmethacrylate (500 mm in height and 90 mm in diameter), and an air pressurization chamber. To obtain uniform fluidization of the abrasives in the bed, a distributor with porous plates of 8 mm thickness in sintered bronze was used.

During the experiments, only the minimum amount of air needed to fluidise the abrasives was supplied and a "minimum fluidization rate" was established. Abrasives increase in volume and act as a liquid that surrounds the entire surface of the workpiece. When the fluidised bed is operated in a minimum fluidisation regime, the abrasives move along arbitrary trajectories at a very low speed (i.e. negligible relative to the rotational speed of the workpiece) relative to the fluidisation column wall. The samples were placed 50 mm from the porous plate dispenser. To obtain a homogeneous coating, the samples were rotated inside the fluidised bed, using the electric engine and a locking device, which translates into better uniformity and homogeneity of the coating. The application of the coating takes place through the phenomenon of the embedding, which consists of the fragmentation of brittle powders on aluminium into splinters and subsequent incorporation of the debris formed into the metal surface. As a result, a thin, rapidly growing coating is obtained.

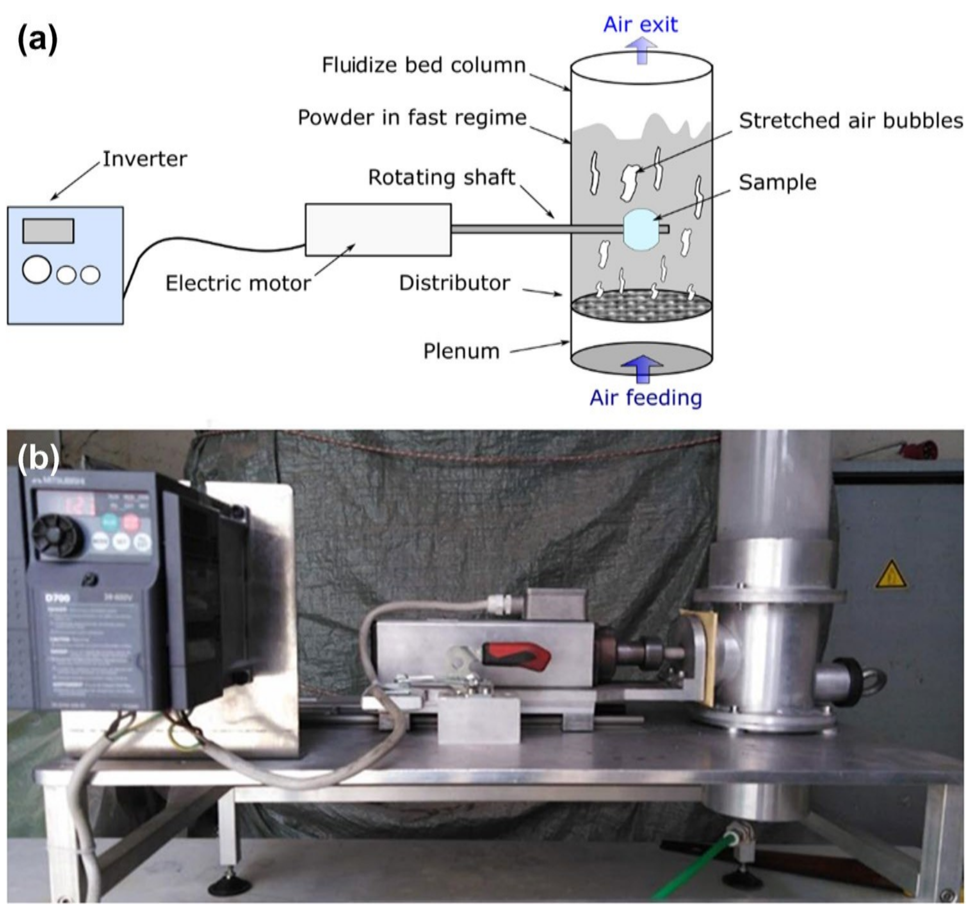

Fig. 3 Schematic (**a**) and experimental setup (**b**) of the fluidised bed device

2.3 Experimental procedures

In order to study the effectiveness of the different treatments, the following superficial treatments on the samples were carried out:

- Surface texturing through laser technology;
- S280 coating using fluidised bed technique;
- Al_2O_3 coating through fluidised bed technique;

In addition, the coated samples were treated in an oven for 1 h at 600 °C and subsequently cooled in water. For fluidised bed coatings, heat treatment was carried out to improve the diffusion of the steel/alumina coating in the aluminium bulk [16]. Samples without any type of treatment were also tested as a reference. Considering also the as-built samples thermally treated and untreated for completeness, a total of 8 different samples replicated 3 times were investigated.

The texture on the samples was performed using the laser system described above, adopting the parameters shown in Table 3; with a high scanning speed (S = 3223 mm/s) laser dots without overlap were produced, while at a lower speed (S = 2100 mm/s) an overlap of approximately 30% was achieved.

Table 3 Parameters used for laser texturing on aluminium samples

Sample	Frequency, f (kHz)	Scanning speed, S (mm/s)	Hatch distance, Hd (mm)
Laser 0%	30	3223	0.105
Laser 30%	30	2100	0.07

In Fig. 4, the images of the surfaces of the samples treated with the laser and their magnification (100 ×) are shown; in the figure, the footprints of each laser pulse are clearly visible. Figure 4a shows the sample with a 30% overlap of the pulses in both directions (vertically and horizontally); while in Fig. 4b, the sample with no pulse overlap (tangent footprints) is reported. The nomenclature used for each analysed sample is shown in Table 4.

The alumina coating was made using the fluidised bed system described above. The treatment was carried out by using alumina balls with a diameter of 1.2–1.4 mm (mesh 16 with a form factor of 0.67) from Smyris Abrasivi S.r.l., for a treatment time equal to 1 h, frequency of the inverter of 16.5 Hz and air pressure of 4 bar.

To obtain the steel coating, steel spheres type S 280, grade 100, with a diameter between 0.6 and 1.18 mm were used. In Fig. 5, the surface images of the steel and alumina-coated samples are shown, in both cases, the average thickness is 10 µm.

Initially, hardness and scratch tests of all the samples were performed by using the Micro-combi tester of the CSM instrument. For the former, a Vickers tip was used for the micro-indentations with a progressive load that reaches a maximum load of 3N. The parameters were chosen according to previous work [16] to observe the influence of the coating on the overall hardness. For each sample typology,

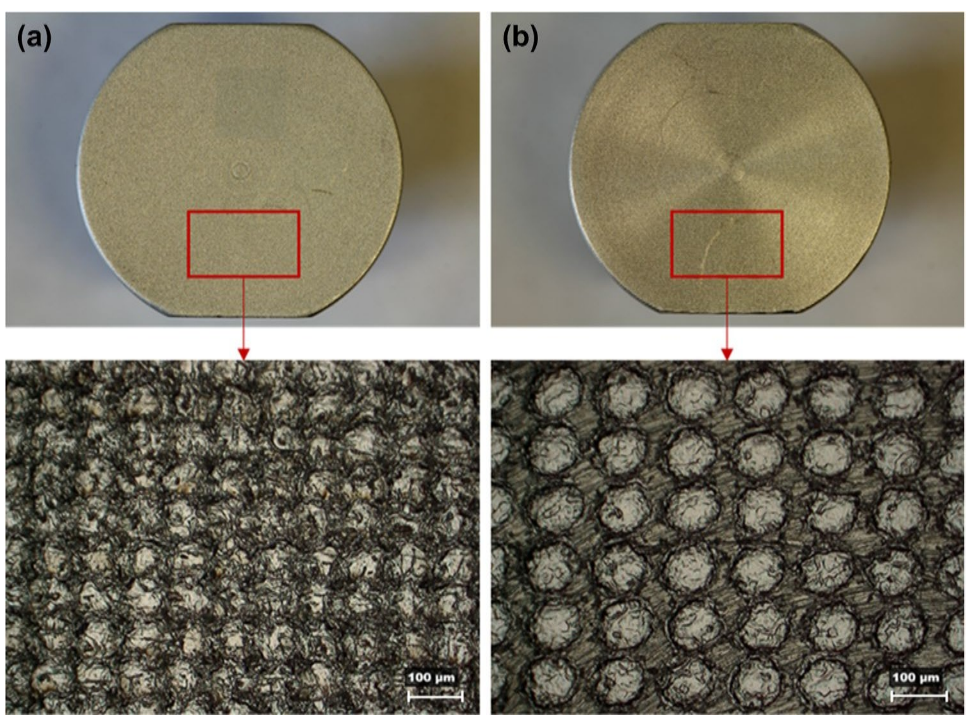

Fig. 4 Surface of the laser textured samples 30% (**a**) and 0% (**b**)

Table 4 Nomenclature of the analysed samples

Sample typology	Sample nomenclature
Untreated sample	As-built
Thermically treated as-built sample	As-built + HT
Alumina coating	Al_2O_3
Thermically treated alumina coating	Al_2O_3 + HT
Steel coating	S 280 steel
Thermically treated steel coating	S 280 steel + HT
Laser treatment with 0% overlap	Laser 0%
Laser treatment with 30% overlap	Laser 30%

14 micro-indentations were made and the mean hardness and standard deviation of each one were calculated. The scratch tests were performed on the samples using a 200 µm Rockwell-C indenter, a 0.30 N progressive load, a track length of 3 mm, and a speed of 1 mm/min. A total of 3 tests were carried out for each sample analysed.

The morphologies of the samples and the roughness parameters were measured with a 3D profilometer Talysurf CLI 2000 by Taylor Hobson, equipped with an inductive probe with a diamond tip (radius of 2 µm). For each sample, 4mm × 4mm maps were acquired with a resolution of 2 µm in-plane directions and a probe velocity of 2 mm/s. In addition, 20 profiles (20 mm length) were acquired for each sample and the main parameters of amplitude and shape roughness (Ra, Rz, RSm, Rsk, Rku, and RΔq) were evaluated in accordance with the ISO 4287: 1997 standard.

The same equipment was adopted to study the scratch tracks: 1.5 mm × 4 mm maps were acquired such as to cover all the traces on the samples, with a resolution of 3 µm on the *x*-axis, and 7 µm on the *y*-axis, with profiles spaced from each other by 7 µm.

To evaluate the hydrophilicity or hydrophobicity of the samples, wettability tests were carried out by calculating the contact angle: a low contact angle ($\theta < 90°$) describes a hydrophilic behaviour, while a high contact angle ($\theta > 90°$) describes a hydrophobic surface. The tests were carried out through the LAUDA LSA 60 machine, by using distilled water released with 3 µml per drop. A total of 3 replicated tests for each sample were performed.

The wear tests on the surface of the samples were carried out using a standard tribometer from CSM Instruments. The counterpart consists of a 6-mm diameter 100Cr6 sphere which moves with a reciprocating motion, the length of the track is equal to 5 mm, and the applied load is 2 N, with a maximum speed of 2.5 cm/s. In total for each sample, 4 wear traces were made at different distances (10 m, 20 m, 60 m, 180 m).

After carrying out the wear tests, the volume of wear removed for each sample was calculated, with the aid of the profilometer described above. Further maps of the wear traces were acquired by covering all the traces on the samples, with a resolution of 3 µm on the *x*-axis, and 7 µm on the *y*-axis, with profiles spaced 7 µm apart from each other.

The cavitation tests have been carried out following a modified ASTM-G32-10 standard [40] used in other works [41–45], with a SONICS VibraCell-505 ultrasonic sonifier, capable of providing frequencies of 20 kHz with adjustable amplitude. The experimental setup is shown in Fig. 6: the samples were immersed in distilled water (300 ml) at a temperature of 25 °C, with a fixed distance from the tip of 5 mm. The amplitude set on the ultrasound processor was 20%.

The total duration of the cavitation tests is 3 h and, at intervals of 30 min, the sample was weighed using a high precision analytical balance (PCE-ABZ 200C by PCE Instruments, with a precision of 0.0001 g) to measure the weight change at regular time intervals. Finally, after completing the cavitation erosion tests, to measure the mass loss for each sample, 3D maps were acquired by using the 3D digital microscopy system (KH-8700 by Hirox).

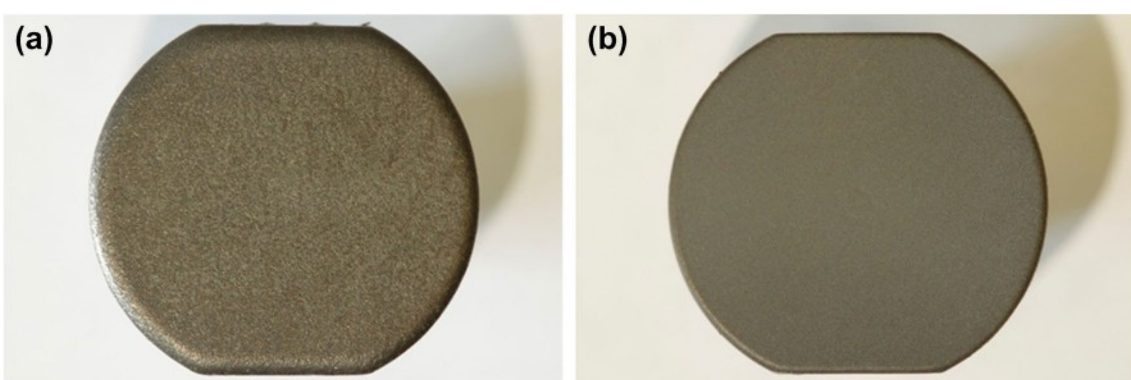

Fig. 5 Fluidised bed coated samples with steel (**a**) and alumina (**b**)

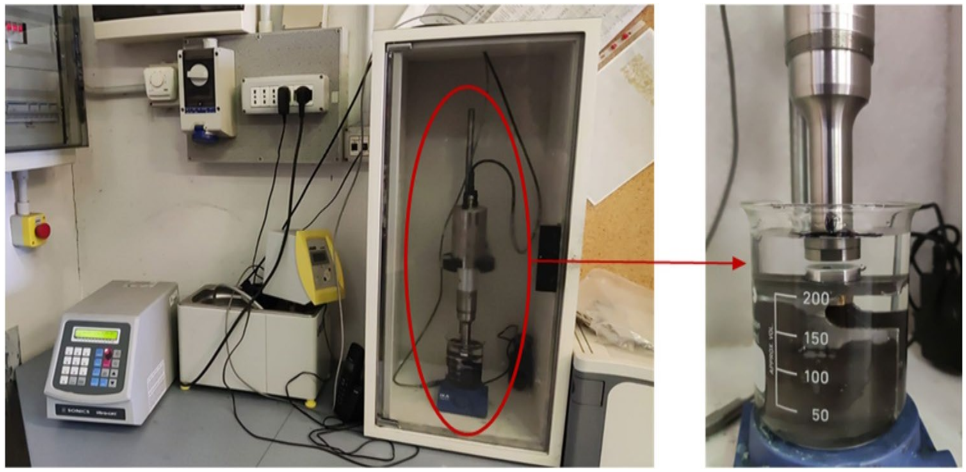

Fig. 6 SONICS VibraCell-505 and detail of the experimental setup of the cavitation tests

3 Experimental results and discussion

3.1 Morphological and mechanical characterisation of the coatings

In the present section, the results relating to the morphological and mechanical characterization tests, in terms of roughness parameters, hardness, scratch resistance, and wettability angle of all types of samples are reported.

The 3D morphological analysis is shown in Fig. 7 and emphasizes the undulations and more generally gives a global view of the tested samples. It can be seen how the treated samples (laser and coated) show a rougher appearance than the surface of the as-built sample. The treatment that gives a more wrinkled morphology is the steel coating made with the fluidised bed technology, due to the higher impact energy of the S280 steel balls, which determines a higher plastic deformation and, thus, a higher morphological variation of the sample, as well as the dimension of the balls. Although, compared to the steel balls, the alumina one show higher dimension, the coating realised with alumina has a lower mass and a higher hardness, characteristics that determine a very different mechanism of formation of the coating: in particular, during impacts, there is a brittle breakage of the alumina on the bulk which, following the plastic deformation of the material, will be incorporated the fragments onto the surface. Since the particles break up are smaller, a more regular and smooth morphology will be obtained. It is worth noting that the heat treatment (1 h at 600 °C) slightly attenuates the surface roughness; this phenomenon can be observed on both the steel and alumina coating. This can be attributed mainly to two different effects based on the coating typology produced: in the case of the steel coating, since the treatment temperature is close to the melting temperature of the bulk material (aluminium), the sinking of the steel coating on the substrate occurs; this is due to the higher mass of the coating. Conversely, in the alumina coating, the mass variation is lower, and the morphological differences can be attributed to the diffusion phenomena. This behaviour is confirmed by the results of the EDS analysis performed in previous work [46], where Al_2O_3 coatings characterised at different treatment temperatures showed an increase in the diffusion of alumina into the bulk as the treatment temperature increased.

Furthermore, it is worth considering that the deposition in the fluidised bed determines a state of compressive stress on the bulk material: the thermal treatment takes the stress relieving; the latter will result in plastic deformation, which influences the overall morphology. This aspect is relevant in the case of the steel coating, which, has higher residual stresses than alumina, and will undergo a greater morphological variation due to the relaxation of residual stresses after the heat treatment.

These results obtained from the morphological analysis are confirmed by the roughness parameters shown in Fig. 8. The main amplitude parameters (Ra and Rz) are approximately quadrupled, comparing the steel deposition and the 0% laser treatment to the as-built sample, while the amplitude parameters closest to the as-built ones are those relating to the alumina coating. Also, comparing the amplitude parameters for both coated samples can be notable that the steel coating has values that are more than twice as alumina (i.e. Ra = ~1.20 μm vs 0.5 μm; Rz = ~8 μm vs 4 μm). The same considerations can be drawn in the case of Rsm. As for laser treatments, the texture of the laser pulses modifies the surface's geometry and consequently the sample's morphological parameters. Regarding the shape parameters, the greatest deviations occur for laser treatments, even if the Rsk and Rku are comparable with the as-built sample. This can be attributed to the surface modification given by a series of repetitions of the laser footprints, which continue to guarantee surface uniformity. The low skewness values for the fluidised bed coatings can be explained since, during the coating application with this technology, the peaks of

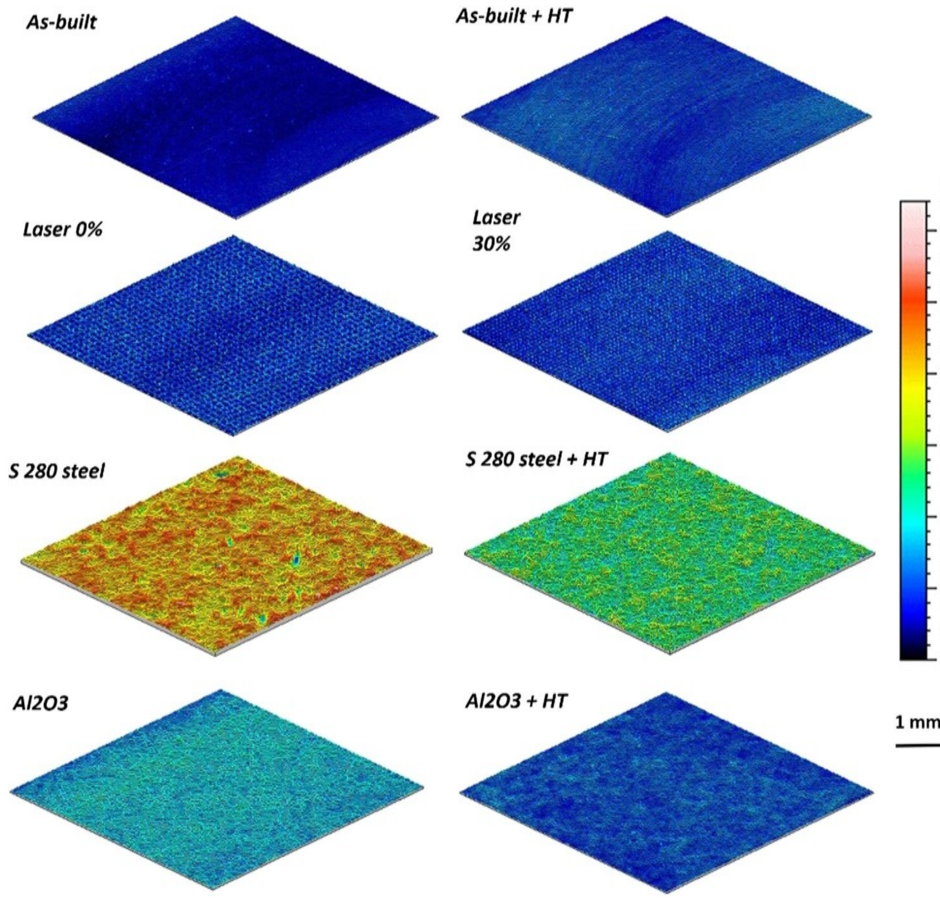

Fig. 7 3D surface morphology of the analysed samples

the bulk and coated material are constantly flattened [39], while the laser technology tends to leave processing burrs.

In Fig. 9, the results of the hardness tests for all the samples are shown. The high hardness of the as-built sample is attributable to the hardening deriving from the turning process. The hardness of both the coated samples results higher than the uncoated ones for different reasons. Firstly, the applied materials (steel/alumina) are harder than the bulk, influencing the measurements. Secondly, there is the hardening of the bulk material, due to the plastic deformation that occurs during the fluidised bed machining. After the heat treatment, due to the hardening stress relieving and grain enlargement underlined with the SEM image shown in Fig. 10 [16], the hardness values are approximately similar for all the treated samples, with values slightly higher in the case of coated samples. The hardness of the laser-treated samples is of the same order of magnitude as the hardness of the samples as-built, indicating that this treatment acts only superficially without changing the internal microstructure of the base material. As for the fluidised bed coatings (both steel and alumina, thermally untreated), these give a greater hardness than the as-built ones. In addition, comparing both laser treatments, the laser with the 30% spot overlap shows a lower value of hardness (i.e. a mean value of 124 HV for the Laser 30% vs 135 for the Laser 0%); this can be attributable to the heat transferred during the superficial process, which causes a major increase of the grain size, thus a reduction of the overall hardness.

The results of the scratch tests are shown in Fig. 11: by analysing the plots of the non-heat-treated samples, it can be seen that they present a similar trend, but in the case of fluidised bed coatings, there are higher maximum penetration depth values. This result is not in agreement with the results obtained from the hardness tests, as the samples analysed have higher hardness values. This discrepancy can be attributable to the coating delamination during the indentation tests. Conversely, for the heat-treated coated samples, the penetration depth is higher compared to the same untreated samples in both cases, indicating a lower hardness, following what was highlighted in the micro-hardness tests.

From these reasons, it would seem that the heat treatment has resulted in a worsening of the adhesion of the film, but it is notable that the elasticity (which is determined by the distance between the penetration depth and residual depth as mean values of Pd-Rd/Pd) of the heat-treated samples is higher. This greater elasticity of the heat-treated samples causes a minor material removal as the indenter passes, confirming that the treatment was able to promote the diffusion

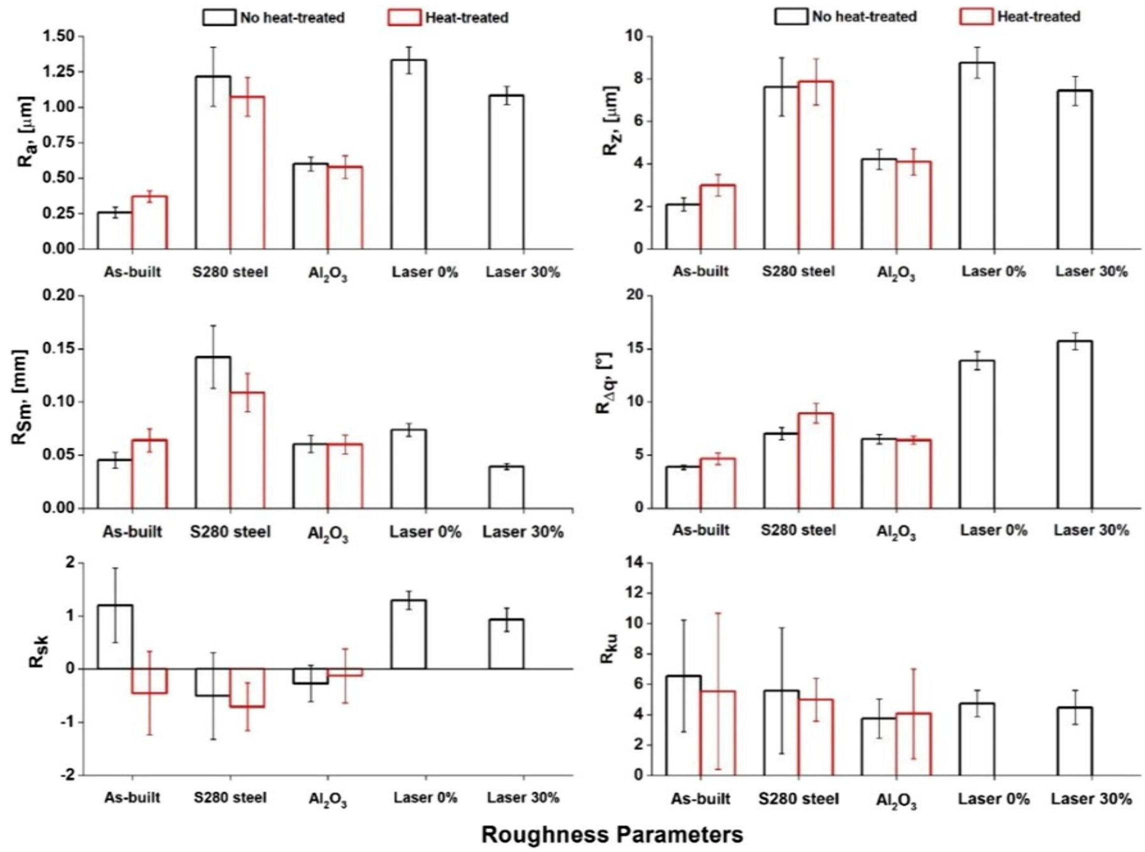

Fig. 8 Roughness parameters computed for the different types of samples analysed

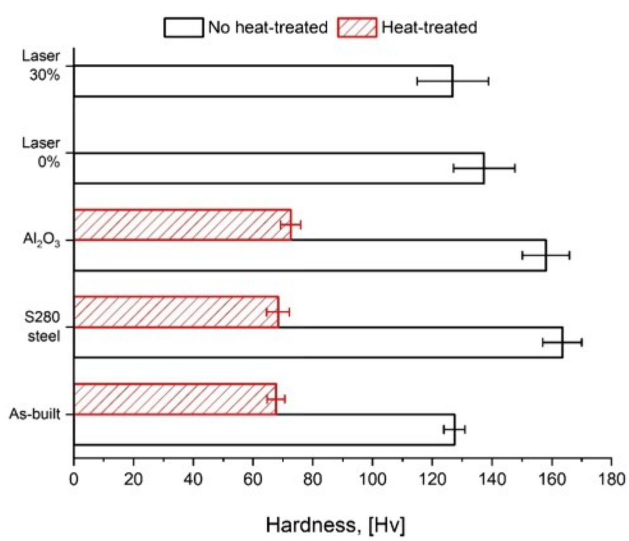

Fig. 9 Hardness of the types of samples analysed

phenomena and, therefore, greater adhesion of the coating. What is proposed is confirmed from the analysis of the 3D maps, which allow underlining that the material accumulation (pile-up) of the heat-treated samples is greater, to highlight a lower removal of the coating.

From the Rd (residual depth) curves shown in Fig. 11 (dashed lines), it can be seen that for all types of samples, there is a final part of the trace in which there is a large pile-up; the latter is greater for the types of thermo-treated samples. This behaviour can be ascribed to the greater ductility of the material and has been verified by making maps of the scratch traces that are shown in Fig. 12. It can be noted that all types of heat-treated samples show a higher material accumulation due to the decrease in hardness with a consequent increase in ductility. Moreover, the steel-coated sample untreated is the one, which shows the lowest material pile-up from the scratch test; this can be attributable to the coating delamination.

As for laser treatments, the Pd (penetration depth) and Rd curves are always greater for the 0% laser treatment than for the 30% laser treatment. This behaviour can be attributable to the different surface morphology: the diameter of the indenter tip is of the same order of magnitude as the surface laser footprints, thus increasing the depth of penetration and elasticity. This behaviour can be explained as in the first type of treatment there is a greater number of peaks and valleys that cause the indenter to spread the peaks of the laser

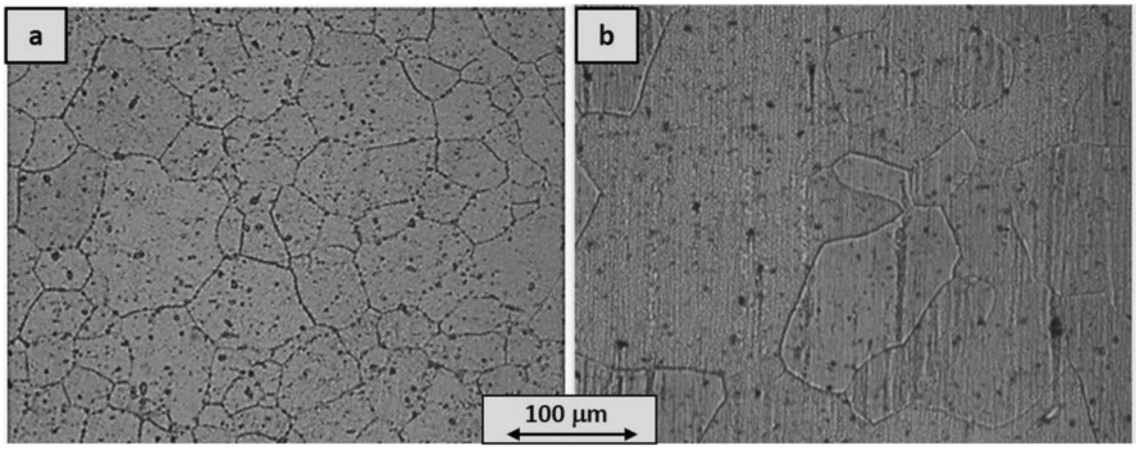

Fig. 10 Grain enlargement obtained after the heat-treatment for the bulk sample

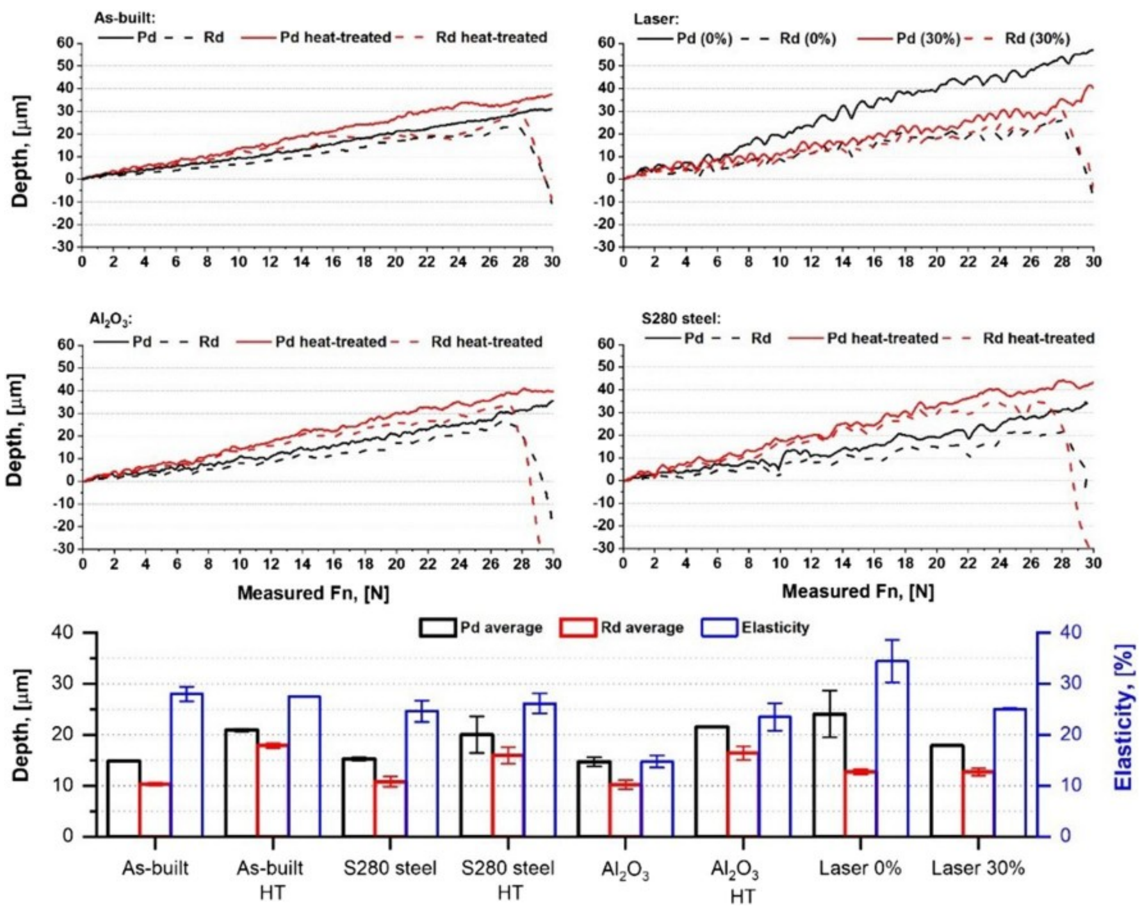

Fig. 11 Scratch test results on the analysed samples

footprint inside the valleys, simultaneously increasing the final pile-up that comes to form.

The measure of wettability of the samples' surfaces was evaluated by measuring the contact angle over time. A greater contact angle indicates a lower wettability of the sample, which is expected to affect both the number of bubbles that impact on the surface, during cavitation. The results of the tests are shown in Fig. 13 and underline how the 0% laser sample is the one showing the lowest wettability, followed by the as-built and 30% laser sample. These results between laser

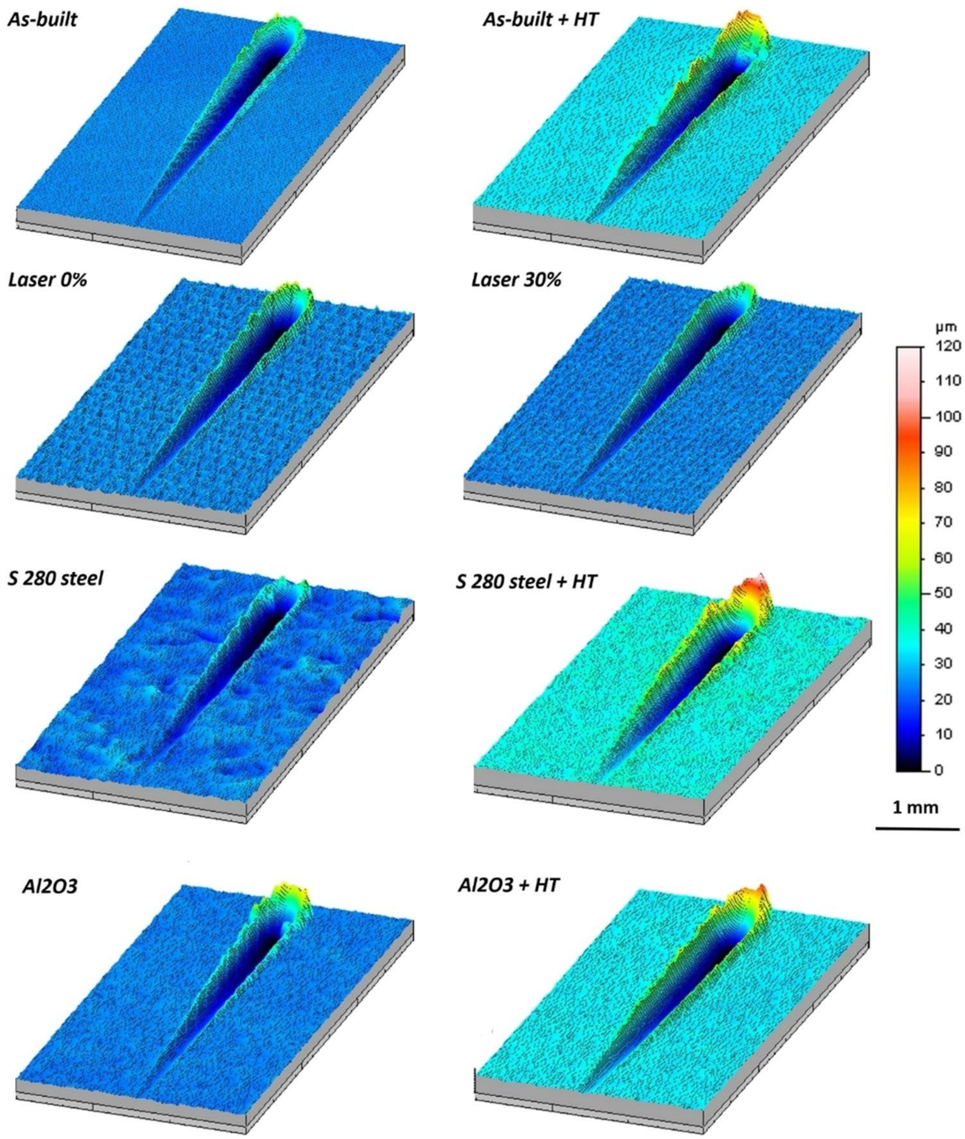

Fig. 12 3D maps of the traces of the scratch tests on the various samples analysed

treatments are consistent with previous work [39]; a surface characterised by a low number and smooth peaks enhances the wettability since the penetration front of the drop spreads all over the substrate surface forming a liquid film. The increasing wettability of all the heat-treated samples may be attributed to the morphology variation and to the increase of oxides on the surface caused by the HT. This is confirmed also by the as-built heat-treated sample, which shows the greatest wettability, i.e. the one showing the lowest contact angle value: since the sample does not have a coating, the increase in wettability can be addicted to the increasing of oxide on the sample surface during the heat treatment.

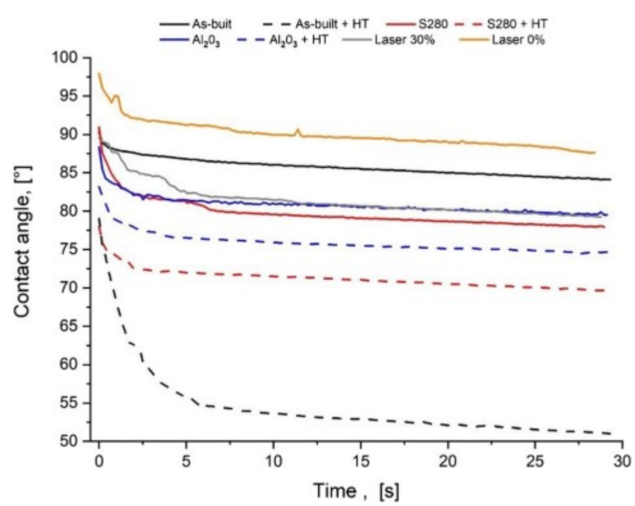

Fig. 13 Evaluation of the wettability of the samples by measuring the contact angle

3.2 Wear test results

The tribological tests were performed as aforementioned, with a load of 2 N and a maximum velocity of 2.5 cm/s.

The wear traces were acquired through the profilometer, and the 3D maps are shown in Fig. 14. The 3D maps show a clear difference between the behaviour of the fluidised bed coated samples compared to the others. In fact, they do not show any damage due to the sliding of the counterpart. This behaviour is to be expected in non-heat-treated samples as they have a higher hardness value (underlined in the hardness tests in Fig. 9). On the contrary, from the heat-treated samples, for the same reason, greater damage is expected but as underlined also during the description of the hardness, in this case, the test took into account also the reduction of the hardness of the bulk material, since the penetration of the indenter was higher than the coating's thickness. This result is consistent with the one obtained from previous work [16] since the heat treatment favoured the diffusion of the coating into the substrate, which improved the adhesion and the wear behaviour. To evaluate numerically the differences between the typologies of produced samples, a calculation of the volume loss during the tests was performed. In particular, Fig. 14 shows the volume loss at different sliding distances (10, 20, 60, 180 m). It can be noted that in heat-treated samples without coating, there is always a deterioration of the wear value for all the sliding distances considered. This behaviour is attributable to the enlargement of the grain in the base material, which has given rise to a clear reduction in the hardness value (from 130 HV to 70 HV).

Regarding laser treatments, 0% shows the largest wear volume; this can be due to surface morphology (Fig. 15): the dots are craters already removed from the surface; this can promote the material removal during the sliding tests.

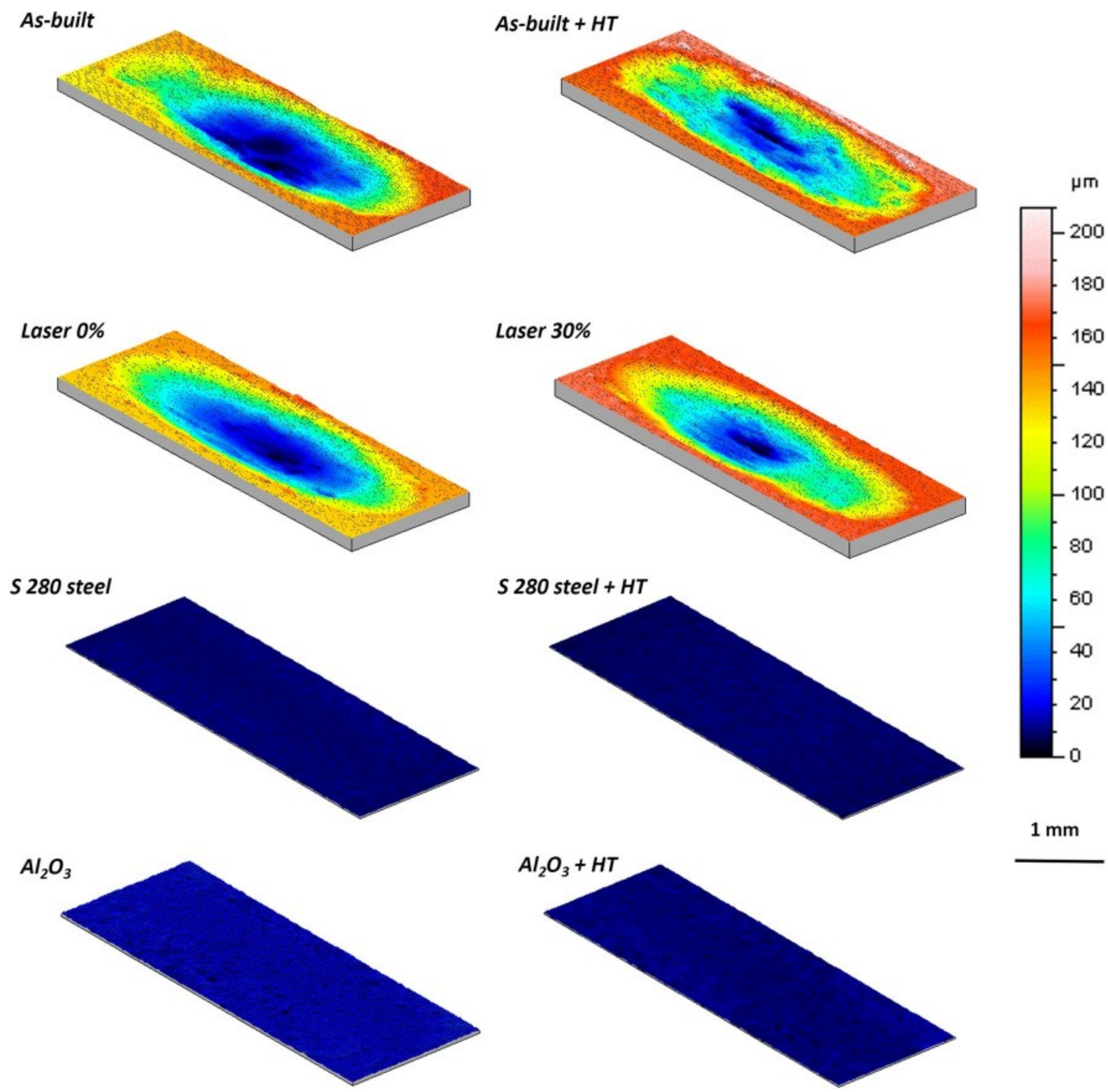

Fig. 14 3D maps of the analysed samples' surface after 180 m of reciprocating wear tests

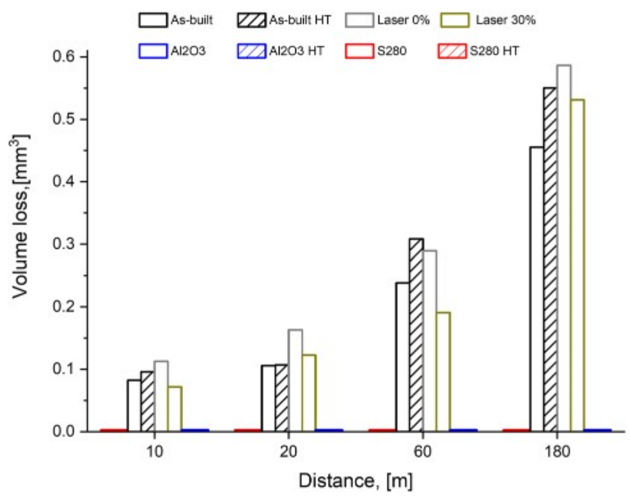

Fig. 15 Volume loss calculated after 10, 20, 60, and 180 m of reciprocated wear tests for all the typologies of treated and untreated samples

Conversely, Laser 30% sample, since shows fewer depressions, the wear is lower and in line with the results obtained for the samples as-built.

3.3 Cavitation tests results

In Figs. 16 and 17, images of the samples after the cavitation test are reported. In the case of the sample as-built, it is notable that the heat treatment is harmful to the purposes of cavitation, with an evident presence of a large number of craters characterized by a greater depth. This behaviour can be attributable to the removal of the surface tensional state of compression and hardening previously induced by the lathing process, by the heat treatment. As a consequence, the sample is mechanically less resistant to cavitation erosion, confirming the results obtained in the hardness and scratch tests.

Concerning fluidised bed coatings, it can be noted that the implosion of bubbles first tends to eliminate the coating, which will act as a protective barrier to the substrate and then acts on the substrate.

The laser treatments show surfaces similar to the samples as-built with extremely localized and regular worn areas, with a reduction of the surface affected by the phenomenon at the same time.

Figure 18 shows the mass losses due to cavitation as a function of the cavitation time. The figure confirms the results of the surface analysis since it is possible to note that the coated samples are the ones that lose the highest mass. It is worth underlining that the mass loss is affected by the density of the coatings: the removal of the coating induces a greater reduction in mass during the test since these coatings are made of heavier materials (alumina/steel). The alumina coating, being lighter than the steel one, but densest than the aluminium, shows lower mass losses and is in line with the losses obtained from the heat-treated as-built.

It is notable that the heat treatment carried out on the samples processed in the fluidised bed initially gave an improvement in the resistance to cavitation erosion compared to the untreated counterparts. This aspect (visible from plots in Fig. 18a) can be attributed to the different erosion mechanism that is established during the test. Initially, the implosion of bubbles tends to remove the coating, which will act as a protective barrier for the substrate;

Fig. 16 Surfaces of the samples as they are and with alumina coating with and without heat treatment after carrying out the cavitation tests with different exposure times

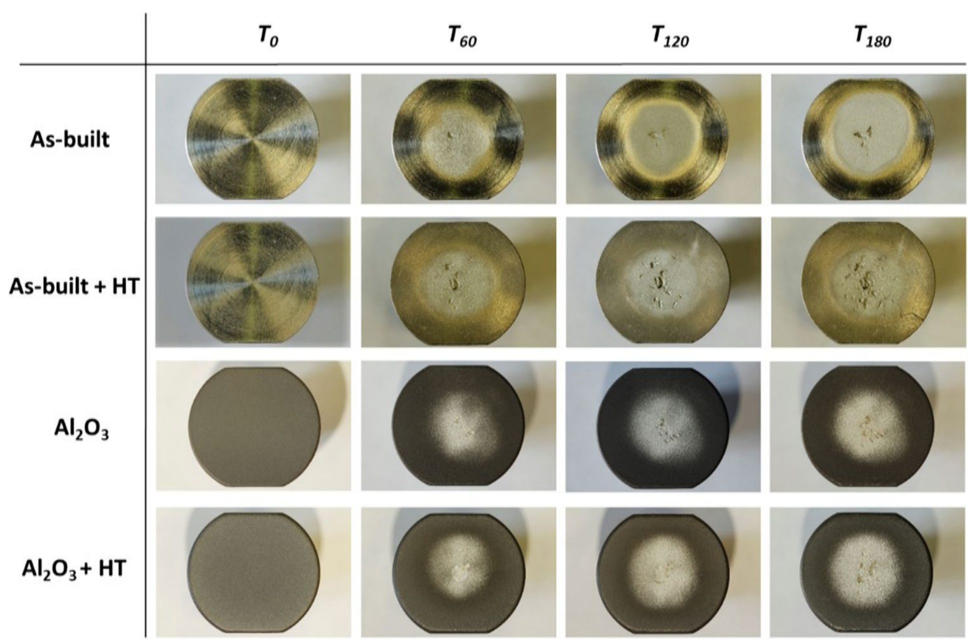

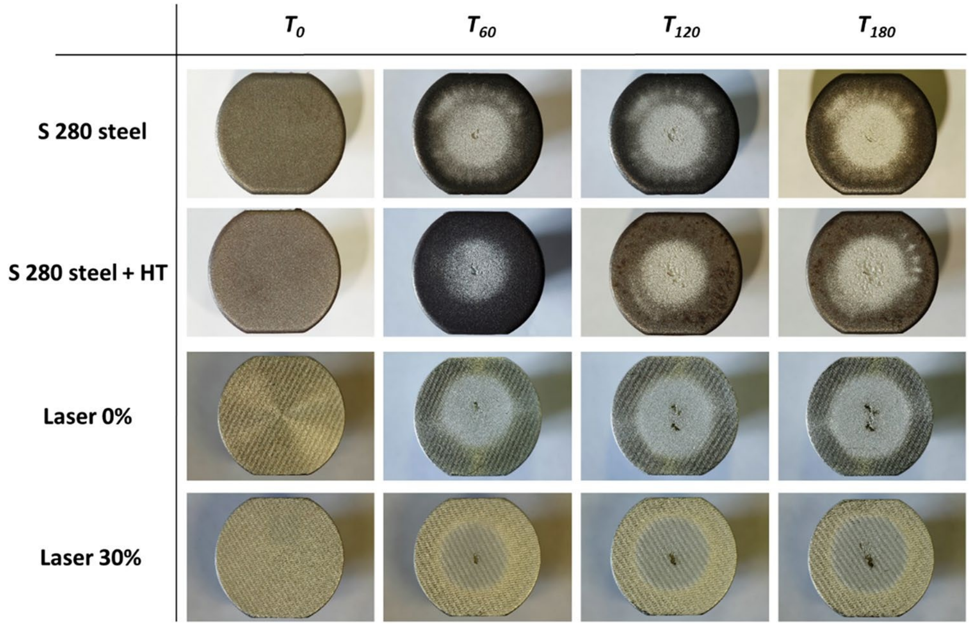

Fig. 17 Surfaces of the samples treated with laser and steel coating with and without heat treatment after having carried out the cavitation tests with different exposure times

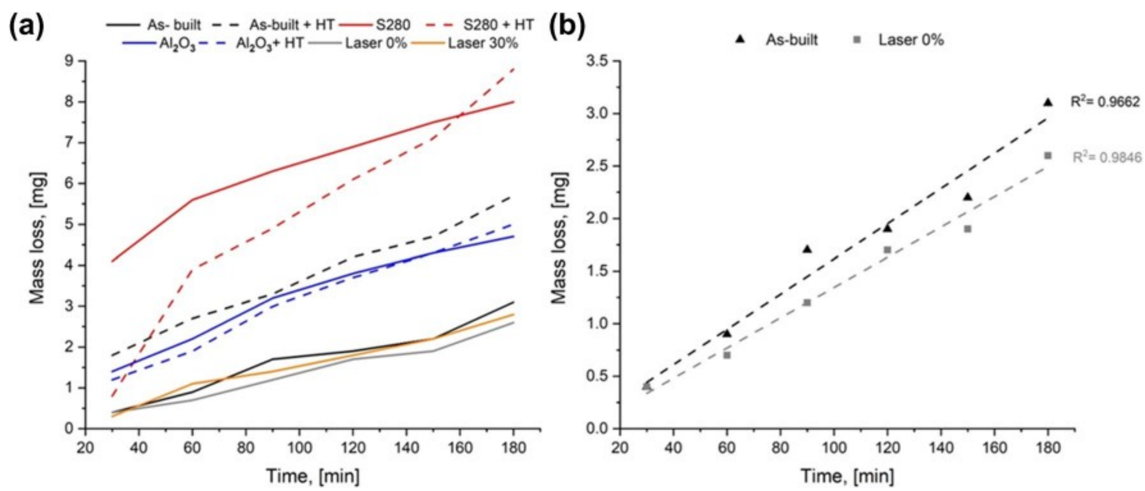

Fig. 18 **a** Mass losses of all samples during cavitation tests at different exposure times. **b** Magnification of the mass losses for the as-built and Laser 0% samples during cavitation tests vs. exposure times

subsequently, once the coating is removed, it starts the removal of the bulk material, which is less resistant due to the absence of the residual compression state (as already highlighted on the sample as-built and heat-treated counterpart). Therefore, the heat treatment effectively determined the diffusion of the coating in the bulk, making it more adherent and improving its cavitation behaviour for up to 150 min. In the last 30 min, there was the removal of the coating and its protective action, thus an accelerated cavitation erosion on the bulk due to the absence of the compressive residual stress.

As for the mass losses obtained from laser treatments, it is clear that these are the least. In particular, the 0% laser treatment shows consistently about 20% lower mass losses than the as-built sample (Fig. 18b). This result is attributable to the surface morphology of the sample: the regular presence of peaks and valleys modifies the type of impact of the bubbles, causing a reduction of erosion due to impacts.

To take into account the difference in density, the evaluation of the worn volume was calculated. Figures 19 and 20 show the volumes and the surface removed after 3 h of cavitation. These results confirm that laser treatments induce lower volume removal, proving to be the most effective type of treatment among those investigated. This can be addicted to the morphology of the surface; according to the literature, the reduction of erosion due to cavitation can be obtained

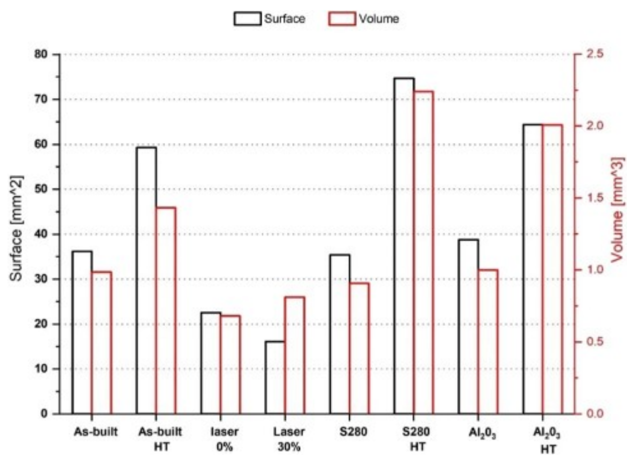

Fig. 19 Evaluation of the areas and volumes removed after 3 h of cavitation test

by applying a modification of the surface, reducing the wettability, thanks to the formation of an air cushion on the surface which can prevent or control corrosion processes [9, 10].

Regarding the heat treatment, even if it increases the diffusion between the different chemical species adopted in the fluidised bed coatings (alumina/steel) [16], it gives the samples lower resistance to the cavitation test; this can be addicted to the stress relieving and the hardness reduction of the surfaces.

4 Conclusions

The main conclusive remarks, which can be drawn from the tests carried out on the samples, are the following:

- Fluidised bed coatings show a homogeneous morphology (overall lower roughness and shape parameters) and greater hardness (in the case of no heat treatment) which imply a better sliding wear behaviour. In the case of heat-treated samples, it should be noted that there is a worse wear behaviour since there is tension relaxation and an increase in the dimension of the grains, but this worsening effect is overcome by the greater diffusion of the coating into the substrate. The diffusion improved the cavitation erosion behaviour of the treated samples compared to their untreated counterpart, indeed, in the initial phase of the tests, when the coating is not totally removed, the overall mass loss is lower.

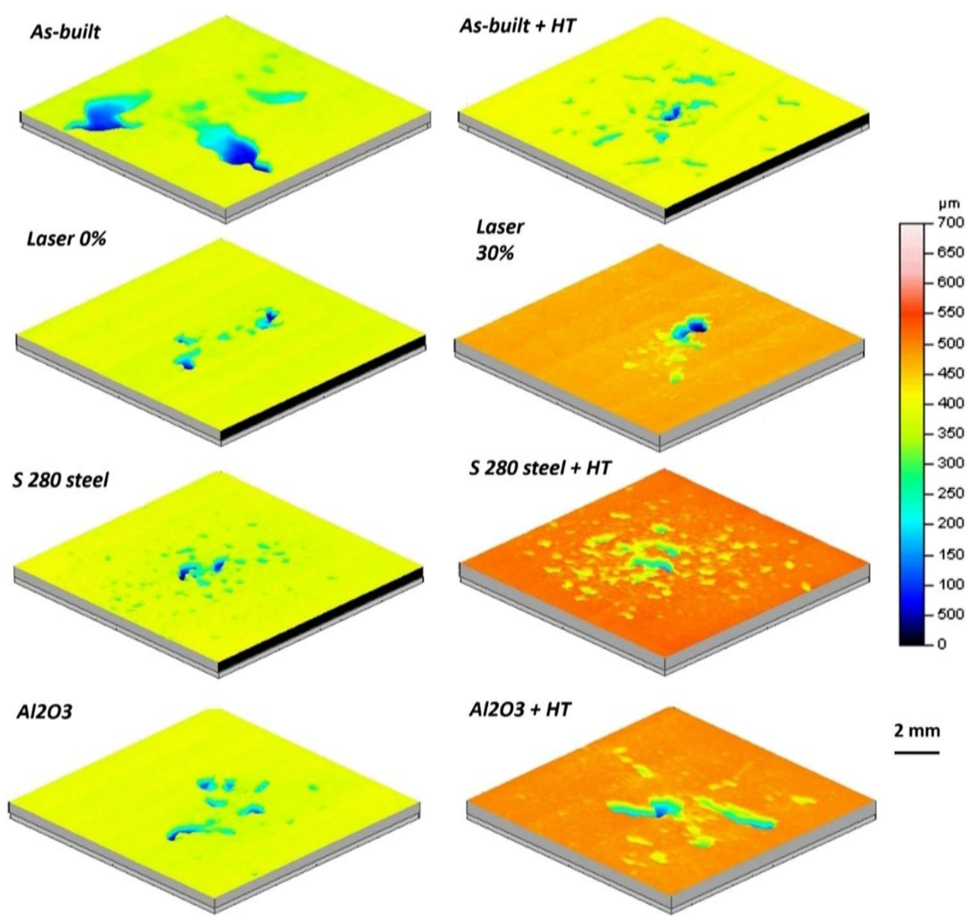

Fig. 20 3D maps of the analysed samples' surface after 3 h of cavitation tests

- Laser treatments reduce cavitation erosion by a maximum of 20% (obtained with the Laser 0% sample); this can be attributed to the variation of the morphology where higher values of Rsk and Rz since higher surface peaks influence the erosion mechanism of the bubbles formed on the surface, thus, a reduction of the wettability of the sample. On the contrary, this type of morphology negatively influences the sliding wear behaviour, since when the contact takes place between the counterpart and the peaks left by the laser imprint, there will be a strong concentration of tensions, increasing the material which will be removed during the test.

It is worth underlining that the fluidised bed coatings work at their best in conditions of sliding wear, meanwhile, the laser treatments are the best ones in terms of cavitation erosion response, so different treatments need to be chosen based on the final application of the alloy.

Acknowledgements The authors are particularly grateful to the Interuniversity Research Centre CIRTIBS for the equipment and the financial support to develop the present research work.

Author contribution SG: conceptualization, investigation, data curation, formal analysis. CL: conceptualization, methodology, formal analysis, resources, supervision. EM: investigation, writing—original draft, data curation, visualization. GR: investigation, data curation, supervision, writing—original draft

Data availability The processed data generated and analysed during the current study are available from the corresponding author upon reasonable request.

Code availability Not applicable.

Declarations

Competing interests The authors declare no competing interests.

Ethics approval Not applicable.

Consent to participate Not applicable.

Consent for publication Not applicable.

References

1. Chowdhury SG, Mondal A, Gubicza J, Krállics G, Fodor Á (2008) Evolution of microstructure and texture in an ultrafine-grained Al6082 alloy during severe plastic deformation. Mater Sci Eng A 490:335–342. https://doi.org/10.1016/J.MSEA.2008.01.049
2. Sabirov I, Yang C, Mullins J, Hodgson PD (2013) A theoretical study of the structure-property relations in ultra-fine metallic materials with fractal microstructures. Mater Sci Eng A 559:543–548. https://doi.org/10.1016/J.MSEA.2012.08.139
3. Karupannasamy DK, SasiKumar KSK, Shankar S (2020) Experimental and numerical analysis of impact strength of Al6082 for automotive structural applications. Mater Today Proc 33:2863–2867. https://doi.org/10.1016/J.MATPR.2020.02.747
4. T.M.A. Bugio, R.F. Martins, L. Leal das Neves, Failure analysis of fuel tanks of a lightweight ship, Eng Fail Anal. 35 (2013) 272–285. https://doi.org/10.1016/J.ENGFAILANAL.2013.01.042
5. Glazoff MV, Khvan AV, Zolotorevsky VS, Belov NA, Dinsdale AT (2019) Industrial and perspective casting alloys. Cast Alum Alloy:405–510. https://doi.org/10.1016/B978-0-12-811805-4.00005-5
6. E. P., P. H.S., T. A., On the mechanisms of cavitation damage and methods of protection, Trans. SNAME. 73 (1965) 241–286.
7. Brassard JD, Sarkar DK, Perron J (2012) Fluorine based superhydrophobic coatings. Appl Sci 2:453–464. https://doi.org/10.3390/APP2020453
8. Hegde M, Mohan J, Warraich MQM, Kavanagh Y, Duffy B, Tobin EF (2023) Cavitation erosion and corrosion resistance of hydrophobic sol-gel coatings on aluminium alloy. Wear 524–525. https://doi.org/10.1016/j.wear.2023.204766
9. Org WE, Zhang K, Wu J, Chu P, Ge Y, Zhao R, Li X (2015) A novel CVD Method for rapid fabrication of superhydrophobic surface on aluminum alloy coated nanostructured cerium-oxide and its corrosion resistance. Int J Electrochem Sci 10:6257–6272 http://www.electrochemsci.org (accessed January 17, 2023)
10. Zhang D, Wang L, Qian H, Li X (2015) Superhydrophobic surfaces for corrosion protection: a review of recent progresses and future directions. J Coatings Technol Res 13(1):11–29. https://doi.org/10.1007/S11998-015-9744-6
11. Shirtcliffe NJ, McHale G, Newton MI, Chabrol G, Perry CC (2004) Dual-scale roughness produces unusually water-repellent surfaces. Adv Mater 16:1929–1932. https://doi.org/10.1002/ADMA.200400315
12. Lau KKS, Bico J, Teo KBK, Chhowalla M, Amaratunga GAJ, Milne WI, McKinley GH, Gleason KK (2003) Superhydrophobic carbon nanotube forests. Nano Lett 3:1701–1705. https://doi.org/10.1021/NL034704T/ASSET/IMAGES/LARGE/NL034704TF00006.JPEG
13. Latthe SS, Imai H, Ganesan V, Rao AV (2009) Superhydrophobic silica films by sol–gel co-precursor method. Appl Surf Sci 256:217–222. https://doi.org/10.1016/J.APSUSC.2009.07.113
14. Latthe SS, Hirashima H, Rao AV (2009) TEOS based water repellent silica films obtained by a co-precursor sol–gel method. Smart Mater Struct 18:095017. https://doi.org/10.1088/0964-1726/18/9/095017
15. Yang T, Tian H, Chen Y (2009) Preparation of superhydrophobic silica films with honeycomb-like structure by emulsion method. J Sol-Gel Sci Technol 49:243–246. https://doi.org/10.1007/S10971-008-1855-4/FIGURES/3
16. Rubino G, Trovalusci F, Barletta M, Fanelli P (2018) Heat treatment of AA 6082 T6 aluminum alloy coated with thin Al2O3 layer by fluidized bed. Int J Adv Manuf Technol 96:2605–2618. https://doi.org/10.1007/S00170-018-1752-0/METRICS
17. Kinoshita H, Ogasahara A, Fukuda Y, Ohmae N (2010) Superhydrophobic/superhydrophilic micropatterning on a carbon nanotube film using a laser plasma-type hyperthermal atom beam facility. Carbon N Y 48:4403–4408. https://doi.org/10.1016/J.CARBON.2010.07.056
18. Han X, Zhang Z, Hou J, Barber GC, Qiu F (2020) Tribological behavior of shot peened/austempered AISI 5160 steel. Tribol Int 145:106197. https://doi.org/10.1016/J.TRIBOINT.2020.106197
19. Martín V, Vázquez J, Navarro C, Domínguez J (2020) Effect of shot peening residual stresses and surface roughness on fretting fatigue strength of Al 7075-T651. Tribol Int 142:106004. https://doi.org/10.1016/J.TRIBOINT.2019.106004
20. Luo KY, Yao HX, Dai FZ, Lu JZ (2014) Surface textural features and its formation process of AISI 304 stainless steel subjected to

massive LSP impacts. Opt Lasers Eng 55:136–142. https://doi.org/10.1016/J.OPTLASENG.2013.10.026
21. Xu G, Lu JZ, Cui CY, Luo KY (2019) Effects of laser shock peening (LSP) on the microhardness, residual stress and microstructure in the weld joint of a stainless steel tube resistance. LIE 43:67–80
22. Jeng YR, Lee JT, Hwu YJ, Liu LC, Lu CY (2020) Effects of operation parameters of cold rolling on surface finish of aluminum. Tribol Int 148:106321. https://doi.org/10.1016/J.TRIBOINT.2020.106321
23. Valiev RZ, Langdon TG (2006) Principles of equal-channel angular pressing as a processing tool for grain refinement. Prog Mater Sci 51:881–981. https://doi.org/10.1016/J.PMATSCI.2006.02.003
24. Mukai T, Yamanoi M, Watanabe H, Higashi K (2001) Ductility enhancement in AZ31 magnesium alloy by controlling its grain structure. Scr Mater 45:89–94. https://doi.org/10.1016/S1359-6462(01)00996-4
25. Saeidi K, Gao X, Zhong Y, Shen ZJ (2015) Hardened austenite steel with columnar sub-grain structure formed by laser melting. Mater Sci Eng A 625:221–229. https://doi.org/10.1016/J.MSEA.2014.12.018
26. Raami L, Varis T, Valtonen K, Wendler M, Volkova O, Peura P (2023) Enhancing the cavitation erosion resistance of AISI 420-type stainless steel with quenching and partitioning. Wear, 526–527. https://doi.org/10.1016/j.wear.2023.204897
27. Astarita A, Genna S, Leone C, Minutolo FMC, Rubino F, Squillace A (2015) Study of the laser remelting of a cold sprayed titanium layer, in: Procedia CIRP, pp 452–457. https://doi.org/10.1016/j.procir.2015.06.101
28. Bonek M (2013) Laser Surface Alloying. Encycl Tribol:1938–1948. https://doi.org/10.1007/978-0-387-92897-5_687
29. F. Rubino, A. Astarita, P. Carlone, S. Genna, C. Leone, F. Memola Capece Minutolo, A. Squillace, Selective laser post-treatment on titanium cold spray coatings, Mater Manuf Process. 31 (2016) 1500–1506. https://doi.org/10.1080/10426914.2015.1037912.
30. Viscusi A, Astarita A, Genna S, Leone C (2018) On the influence of different superficial laser texturing on the deposition of powders through cold spray process. Trans Inst Met Finish 96:34–40. https://doi.org/10.1080/00202967.2018.1403096
31. Genna S, Giannini O, Guarino S, Ponticelli GS, Tagliaferri F (2020) Laser texturing of AISI 304 stainless steel: experimental analysis and genetic algorithm optimisation to control the surface wettability. Int J Adv Manuf Technol 110:3005–3022. https://doi.org/10.1007/S00170-020-06073-4
32. Sexton L, Lavin S, Byrne G, Kennedy A (2002) Laser cladding of aerospace materials. J Mater Process Technol 122:63–68. https://doi.org/10.1016/S0924-0136(01)01121-9
33. Weng F, Chen C, Yu H (2014) Research status of laser cladding on titanium and its alloys: a review. Mater Des 58:412–425. https://doi.org/10.1016/J.MATDES.2014.01.077
34. Tomlinson WJ, Talks MG (1990) Laser surface processing and the cavitation erosion of a 16 wt.% Cr white cast iron. Wear 139:269–284. https://doi.org/10.1016/0043-1648(90)90050-K
35. B.G. Gireń, Cavitation erosion of steels processed with laser beam and optical discharge plasma, Http://Dx.Doi.Org/10.1179/Sur.1998.14.4.325. 14 (2013) 325–330. 10.1179/SUR.1998.14.4.325.
36. Bordeasu I, Popoviciu MO, Micu LM, Oanca OV, Bordeasu D, Pugna A, Bordeasu C (2015) Laser beam treatment effect on AMPCO M4 bronze cavitation erosion resistance. IOP Conf Ser Mater Sci Eng 85:012005. https://doi.org/10.1088/1757-899X/85/1/012005
37. Man HC, Kwok CT, Yue TM (2000) Cavitation erosion and corrosion behaviour of laser surface alloyed MMC of SiC and Si3N4 on Al alloy AA6061. Surf Coatings Technol 132:11–20. https://doi.org/10.1016/S0257-8972(00)00729-5
38. Kwok CT, Man HC, Cheng FT (1998) Cavitation erosion and pitting corrosion of laser surface melted stainless steels. Surf Coatings Technol 99:295–304. https://doi.org/10.1016/S0257-8972(97)00624-5
39. Ponticelli GS, Tagliaferri F, Genna S, Venettacci S, Giannini O, Guarino S (2021) Soft computing techniques for laser-induced surface wettability control. Mater 14:2379. https://doi.org/10.3390/MA14092379
40. ASTM (2021) G32-16 - Standard test method for cavitation erosion using vibratory apparatus. ASTM Int.:1–19 https://www.astm.org/g0032-16r21e01.html (accessed January 18, 2023)
41. Fahim J, Hadavi SMM, Ghayour H, Hassanzadeh Tabrizi SA (2019) Cavitation erosion behavior of super-hydrophobic coatings on Al5083 marine aluminum alloy. Wear 424–425:122–132. https://doi.org/10.1016/J.WEAR.2019.02.017
42. Song QN, Xu N, Bao YF, Jiang YF, Gu W, Zheng YG, Qiao YX (2017) Corrosion and cavitation erosion behaviors of two marine propeller materials in clean and sulfide-polluted 3.5%NaCl solutions. Acta Metall Sin. English Lett 30:712–720. https://doi.org/10.1007/S40195-017-0602-7/FIGURES/8
43. Tang CH, Cheng FT, Man HC (2004) Improvement in cavitation erosion resistance of a copper-based propeller alloy by laser surface melting. Surf Coatings Technol 182:300–307. https://doi.org/10.1016/J.SURFCOAT.2003.08.048
44. Basumatary J, Nie M, Wood RJK (2015) The synergistic effects of cavitation erosion–corrosion in ship propeller materials. J Bio- Tribo-Corrosion 1:1–12. https://doi.org/10.1007/S40735-015-0012-1/TABLES/5
45. Atzeni E, Genna S, Menna E, Rubino G, Salmi A, Trovalusci F (2021) Surface finishing of additive manufactured ti-6al-4v alloy: a comparison between abrasive fluidized bed and laser finishing. Materials (Basel) 14. https://doi.org/10.3390/MA14185366
46. Baiocco G, Rubino G, Ucciardello N (2019) Heat treatment of AZ91 magnesium alloy coated with an Al2O3 thin film with fluidized bed technology. Materials 12:216. https://doi.org/10.3390/ma12020216